Finite-Volume and Integral-Equation Techniques for Transonic and Supersonic Vortex-Dominated Flows

ICAS-86-1.5.4

Osama A. Kandil*, Andrew Chuang** and Li-Chuan Chu**
Department of Mechanical Engineering and Mechanics
Old Dominion University, Norfolk, VA 23508, USA

Abstract

Two computational techniques are developed to calculate the compressible vortex-dominated flows. The first technique is a finite-volume Euler Solver which uses four-Stage Runge-Kutta time stepping with second - and fourth-order dissipation terms. The technique is applied to supersonic conical and three-dimensional flows about sharp - and round-edged delta wings. Attached and separated-flow solutions have been obtained depending on the values of damping coefficients. The second technique is an integral-equation solver of the full potential equation which uses a volume-integral term in addition to the classical surface-integral terms. The technique is applied to transonic three-dimensional flows about sharp-edged delta wings. A hybrid technique which combines the finite-volume and the integral-equation solvers is also presented.

Introduction and Background

Prediction of the flow field around highly swept delta and delta-like wings is still a challenging problem to the computational fluid dynamics community. As it is well known, the flow field is strongly dependent upon the angle of attack (α) , the sweep back angle (β) and the free-stream Mach number (M_∞) . The number of variables is reduced by one if the normal angle of attack (α_N) and the normal free-stream Mach number (M_N) are used, instead of α, β and M_∞ , to describe the flow field dependence. The new variables α_N and M_N are given by the simple geometric relationships

$$\alpha_N = \tan^{-1} (\tan\alpha/\cos\beta) \qquad (1)$$

$$M_N = M_\infty \cos\beta \, (1 + \sin^2\alpha \, \tan^2\beta)^{1/2} \qquad (2)$$

In the early 60's, Stanbrook and Squire[1,2] classified the flow field about sharp-edged delta wings according to α_N and M_N into two main types - a flow with leading-edge separation and a flow with an attached flow at the leading-edge. In Figure 1, the former type of flow is referred to by region (A) and the latter type of flow is referred to by regions (B) and (C). In region (A), the flow separates at the leading edge (primary separation) and rolls up into a leading-edge vortex core which creates a suction-pressure peak on the wing upper surface with an adverse spanwise pressure gradient. The outboard, spanwise, boundary-layer flow on the upper surface separates due to the adverse spanwise pressure gradient forming a secondary separation and causing, for laminar-boundary layer flows, another suction peak in the spanwise pressure distribution. Depending on the flow conditions, tertiary separation may develop on the outboard side of the secondary point of separation.

In regions (B) and (C), a detached or an attached bow shock is formed upstream of the leading edge, the flow is attached at the leading edge, and supersonic flow expansions occur ending with an inboard conical shock. Depending on the shock strength, shock induced separation may develop on the inboard side of shock.

The Stanbrook-Squire diagram was modified by Vorropoulos and Wendt[3] who introduced subregion (A_1) within region (A) where a conical shock was observed on the suction side under the leading-edge vortex. The flow in this region, between the wing surface and the lower surface of the leading-edge vortex, is analogous to the flow in a convergent-divergent channel where the accelerated supersonic flow ends with a shock. Again depending on the shock strength, a shock induced separation may develop on the outboard side of the shock. This subregion corresponds to high-subsonic M_N and moderate α_N .

At the same time, Miller and Wood[4,5] expanded the Stanbrook-Squire diagram through an extensive experimental research program. Depending on M_N and α_N , they classified the flow into seven regions as shown in Figure 2. In addition to the flows described above, leading-edge separations with shock waves above the leading-edge vortex are also possible flows for subsonic and supersonic M_N at large α_N .

It is obvious that we are dealing with a very complex flow field which may include a leading-edge separation with a secondary separation, an attached leading-edge flow with an inboard shock and a possible shock-induced separation, or a combination of the leading-edge separation and the inboard shock with secondary and shock-induced separations. The complexity of the flow field increases at large angles of attack when the leading-edge vortex core breaks down over the wing. The ultimate complexity of the flow field is reached during maneuverability

* Professor
** Graduate Research Assistant

where the flow field will change from one region to the other along with the effects of time history of the flow.

In the computational area, a substantial volume of research work has recently been and is still being produced by several investigators to accurately predict certain types of the many complex types of flow fields presented above. These prediction techniques are based on the full potential equations[6-8], the Euler equations[9-23] and the Navier-Stokes equations[24-28]. In reference 6, the integral equation solution has been used through a modified nonlinear discrete-vortex technique for the incompressible flow to show the roll-up process of the trailing-edge vortex into a trailing-edge vortex core and its interaction with the leading-edge vortex core. For a delta wing of sweep back angle of 76° at an angle of attack of 20.5°, it has been shown that the trailing-edge vortex core is fully formed within a quarter of a chord length behind the trailing edge and that the process can be predicted by an inviscid technique. Higher-order modeling of the separated flow using local linear vorticity distribution has been introduced in reference 7 for the steady and unsteady incompressible flow and accurate flow prediction has been obtained. This is followed by attacking the steady transonic-vortex dominated flows[8] using the integral-equation solution which includes a volume integral term representing the full flow compressibility. The technique is applied to predict the experimental subregion (A_1) which was observed by Vorropoulus and Wendt[3].

The steady Euler equations have been used to calculate the supersonic flows around sharp-edged delta wings with leading-edge separation[9,10] while the unsteady Euler equations have been used to calculate the steady transonic[11-13] and supersonic[15-23] flows around sharp[11-18,20-23] and round-edged[17-21] delta wings. For the transonic regime, the computed surface pressure has been dissatisfactory[11-13] since the suction-pressure peak was underpredicted and substantially shifted toward the leading edge. Although some researchers believe that the problem behind the predicted location of the suction-pressure peak is due to the inability of Euler equations, since they are inviscid equations, to predict the secondary separation, we strongly believe that the problem is due to the diffusive effect of the numerical dissipation. It should be recalled that the predicted surface pressures using the panel techniques (inviscid techniques) compared well with the measured surface pressures where turbulent-boundary layer flows were maintained on the wing surface and hence the secondary separation had the minimum effect on the surface pressure.

From our experience with FL057 for this range of Mach numbers 0.7-0.85, it has been concluded that the dissipation terms, along with the type, fineness and boundaries of the grids are the main reasons for this disappointing prediction. It should be pointed out here that the second-order dissipation terms reach their maximum values in regions of high pressure gradients which include not only shocks but also vortical flows. One cure for this problem, instead of refining the grid, is to shield most of the vortical flow from the numerical dissipation effect by splitting the flow vector field into two components; one due to the vortical flow and the other due to the remaining disturbances in the flow. The former is calculated from the integral equation solver[8] while the latter is calculated from the Euler-equation solver[21].

For the supersonic regime with leading-edge separation, the leeward suction-pressure peak is not as high as that of the subsonic and transonic flows since the leading edge vortex is flattened and hence the flow is less dominated by the vortex flow as compared to that of the subsonic and transonic flows. The diffusive effect of the numerical dissipation on the vortical flow is not severe and the prediction of the surface pressure for sharp-edged delta wings using the Euler equations is better[16-18,20-23] than that for subsonic and transonic flows.

It is very interesting here to mention that for supersonic conical flow solutions of sharp-edged wings, Murman and his co-workers[15,16,22] are reporting agreement of the computed total pressure losses, irrespective of the level of dissipation, with the measured ones. Although we obtained similar results using a similar finite-volume Euler solver, we are careful not to claim at the time being that Euler equations solutions are satisfactory to predict these viscous flow phenomena, such as the total pressure losses and vortex breakdown, until the effects of numerical dissipation are completely resolved.

Solutions for supersonic conical flows have recently been presented for sharp-edges[15-18, 20-23] and for round-leading edges[17-21]. Using Euler solvers for sharp-edged wings, coarse and fine grids gave consistent solutions[17,18,20,21] while for round-edged wings coarse and fine grids gave inconsistent solutions[17-21]. By inconsistent solutions we mean separated and attached flow solutions. In particular, Newsome and Thomas[18] have shown that coarse and fine grids using McCormack's unsplit, explicit, finite-difference algorithm give inconsistent solutions while upwind solutions using the flux vector splitting algorithm are consistent. In reference 19, Chakravarthy and Ota have shown, for the same round-edged wing used by Newsome and Thomas, that a very coarse grid using upwind TVD scheme gives inconsistent solutions with global minimum time stepping and with local time stepping. Although Newsome and Thomas believe that the main reason behind the inconsistent solutions is the grid coarseness, Chakravarthy and Ota believe that it is due to the use of local time stepping.

In reference 20 and 21, it has been shown that separated supersonic conical flow solutions are obtained for sharp-edged delta wings

irrespective of the level of dissipation (as long as it is sufficient to produce a stable solution) or the grid fineness. For round-edged delta wings, it has been shown that separated-and attached-flow solutions, using coarse grids, are dependent on the level of dissipation. It has been also shown that the solution for round-edged wings is independent of the way time stepping is done - local and global-minimum time stepping produce the same solution.

Solutions for supersonic locally-conical [17,18] and three-dimensional [25-27] flows and for subsonic and transonic three-dimensional flows [24,28] have been obtained using the Navier-Stokes equations. For large Reynolds number flows, fine grids and the corresponding large computational time are still major problems in using the Navier-Stokes solvers. In subsonic and transonic flow applications, diffusive effects of the numerical dissipation have also been reported in reference 28.

In this paper, we review the integral equation approach for transonic vortex-dominated flows and the finite-volume Euler solver for supersonic conical and three-dimensional vortex-dominated flows. Additional results are reported for the Euler solver at very high angles of attack where shocks have been captured above and below the leading-edge vortex depending on the free-stream Mach number. Also, detailed results for three-dimensional supersonic flow are presented and compared with the conical supersonic solution. A hybrid technique which combines the Euler and integral-equation solvers, to reduce the effects of numerical dissipation, is also presented.

Integral-Equation Solver

Formulation

The governing equations of the three-dimensional, steady, compressible, potential flow around a wing are given by

$$\Phi_{xx} + \Phi_{yy} + \Phi_{zz} = G \tag{3}$$

$$\rho = \left[1 - \frac{\gamma-1}{2} M_\infty^2 (1 - u^2 - v^2 - w^2)\right]^{1/\gamma-1} \tag{4}$$

$$G = -\frac{1}{\rho} (\rho_x u + \rho_y v + \rho_z w) \tag{5}$$

where Φ is the total velocity potential, ρ is the density, γ is the ratio of specific heats, M_∞ is the free-stream Mach number and u, v, w are the velocity components of the total velocity $\bar{V}$ which is given by the Helmholtz decomposition

$$\bar{V} = \Delta\Phi + \bar{V}' \tag{6}$$

where $\bar{V}'$ is the solenoidal velocity due to the rotational flow. It should be noticed that equation (3) is obtained from the continuity equation using the solenoidal property of $\bar{V}'$, $\nabla \cdot \bar{V}' = 0$.

The formal integral solution to equation (3) in terms of the velocity field is substituted into equation (6) to obtain the total velocity at any field point p

$$\bar{V}_p(x,y,z) = \bar{e}_\infty + \frac{1}{4\pi} \oint\!\!\oint_g \frac{q}{r^2} \bar{e}_r \, ds + \frac{1}{4\pi} \oint\!\!\oint_g \frac{\bar{\omega}(\xi,\eta,\zeta) \times \bar{r}}{r^3} ds + \frac{1}{4\pi} \oint\!\!\oint_w \frac{\bar{\omega}(\xi,\eta,\zeta) \times \bar{r}}{r^3} ds + \frac{1}{4\pi} \iiint \frac{G(\xi,\eta,\zeta)}{r^2} \bar{e}_r \, d\forall \tag{7}$$

where p(x,y,z) is a field point, $\bar{e}_\infty$ is a unit vector in the free-stream direction, the subscripts g and w refer to the wing and free-vortex-sheet surfaces, respectively; q is a surface source distribution, $\bar{\omega}$ is the vorticity; ξ, η, ζ are the coordinates of a source point, $r = [(x-\xi)^2 + (y-\eta)^2 + (z-\zeta)^2]^{1/2}$, G is a source distribution in the flowfield. For a zero-thickness wing, the second term on the right-hand side of equation (7) drops out. Note that the third term does not have to be a surface integral of vorticity since a surface integral of doublets can be equivalently used instead. The fourth term represents the contribution to the velocity field due to the free-vortex sheets emanating from the wing separation lines. Also, this term can be read as $\bar{V}'$ since the vorticity region is lumped into free-vortex sheets. The last term is a volume integral term representing the total compressibility in the flow.

Note that the integrand of the volume integral of equation (7) decreases rapidly with increasing distance from the wing/vortex system not only because of the factor $(1/r^2)$ but also because G diminishes rapidly with increasing distance. Consequently, for computational purposes, the volume integral needs to be addressed only within the immediate vicinity of the wing/vortex system. This is one of the major advantages of the integral equation solvers.

Shock-Capturing Technique

In the shock-capturing technique, equation (7) is iteratively solved to satisfy the flow tangency condition on the wing, Kutta condition along the separation edges, and the flow-tangency condition and no-pressure-jump condition on the free-vortex sheets. The components of the density gradient ρ_x, ρ_y and ρ_z of the compressibility term G are calculated using a backward/central finite-difference scheme. Backward differencing is used at supersonic points while central differencing is used at subsonic points. Details of the computational technique are given in reference 8.

Application to Transonic Vortex-Dominated Flows

We consider a delta wing with aspect ratio of 1.5, angle of attack of 15°, and a free-stream Mach number of 0.7. This case has also been considered by Rizzi and his co-workers in references 11 and 13 through a finite-volume Euler code which uses an O-O transfinite grid consisting of 65x30x42 and 16x49x81; respectively. Figure 3 shows the computed leading- and trailing-edge free-vortex lines and inviscid vortex cores in two- and three-dimensional views.

In Figure 4, we show the spanwise surface pressure variation at a chord station of 0.8. On the same figure, we compare the surface pressure computed by the present method with those computed by Rizzi[11] and the authors using FL057. We also include the experimental data used by Rizzi[11]. It is obvious that the present method compares favorably with the experimental data while the Euler solver substantially underpredicts the suction-pressure peak and mispredicts the location of the leading-edge vortex core. Even with the recent fine grid[13], one million grid points, prediction of the leading-edge vortex core did not improve. Similar disappointing results have been reported earlier by Raj and Sikora[12].

Figure 5 shows the cross-flow velocity and the free-vortex sheets for the same wing behind the trailing edge in planes normal to the wind direction. It is seen that the trailing edge vortex core is fully formed at almost a quarter of a chord length behind the trailing edge.

Figure 6 shows the spanwise variation of the axial velocity in the flowfield through the shock at a chord station of 0.7 for a delta wing of aspect ratio of 1, angle of attack of 20.5°, and free-stream Mach number of 0.8. It is obvious that a curved shock exists and is captured.

Work in Progress

Currently, we are replacing the calculation of the third and fourth terms of equation (7) by the newly developed nonlinear hybrid vortex method which uses an exact set of equations and a bilinear local vorticity distribution. A shock capturing-shock fitting technique, which was developed for two-dimensional flows, is added in the three-dimensional flow problems to sharpen the shock.

Euler-Equations Solver

Formulation

The conservation form of Euler equations for three-dimensional unsteady, compressible flow without external heat addition is

$$\frac{\partial q}{\partial t} + \frac{\partial E}{\partial x} + \frac{\partial F}{\partial y} + \frac{\partial G}{\partial z} = 0 \qquad (8)$$

where the flow vector field q and the fluxes E, F and G are given by

$$q = [\rho,\ \rho u,\ \rho v,\ \rho w,\ \rho e]^t$$

$$E = [\rho u,\ \rho u^2 + p,\ \rho uv,\ \rho uw,\ \rho uh]^t$$

$$F = [\rho v,\ \rho uv,\ \rho v^2 + p,\ \rho vw,\ \rho vh]^t \qquad (9)$$

$$G = [\rho w,\ \rho uw,\ \rho vw,\ \rho w^2 + p,\ \rho wh]^2$$

In equation (9), the density is ρ, the velocity components are u, v, w; the pressure is p and the total energy and enthalpy per unit mass are given by $e = p/\rho(\gamma-1) + (u^2 + v^2 + w^2)/2$ and $h=e + p/\rho$, respectively, where γ is the gas index.

For steady supersonic flows, equations (8) and (9) are simplified by assuming conical flow field. Introducing the conical coordinates defined by

$$\xi = x,\ \eta = y/x,\ \zeta = z/x \qquad (10)$$

in equation (8), we obtain

$$x\frac{\partial q}{\partial t} + \frac{\partial \hat{F}}{\partial \eta} + \frac{\partial \hat{G}}{\partial \zeta} + 2E = 0 \qquad (11)$$

where

$$\hat{F} = F - \eta E \text{ and } \hat{G} = G - \zeta E \qquad (12)$$

The time stepping technique yields, upon reaching a steady flow, self-similar conical solutions. Equation (11) is solved at x=1. The basic finite-volume equation is obtained by integrating equation (11) at x=1 over η and ζ

$$\iint \frac{\partial q}{\partial t}\, dA + \oint (\hat{F}\, d\zeta + \hat{G}\, d\eta) + 2\iint E\, dA = 0 \qquad (13)$$

Computational Scheme

Equation (13) is applied at each cell of a body-conformed grid which is obtained by using a modified Joukowski transformation. The resulting difference equation is given by

$$\left(\frac{\partial q}{\partial t}\right)_{j+1/2,\ k+1/2} \Delta A_{j+1/2,\ k+1/2} + \sum_{r=1}^{4} (\hat{F}_r\, \Delta\zeta_r + \hat{G}_r\, \Delta\eta_r) + 2\, E_{j+1/2,k+1/2}\, \Delta A_{j+1/2,k+1/2} = 0 \qquad (14)$$

where ΔA is the cell area, r refers to the cell-side number and the half-integer subscript refers to the centroidal value. Second- and fourth-order dissipation terms, as proposed by Jameson[21], are added to equation (14). The level of dissipation is changed by varying the values

of the damping coefficients ϵ_2 and ϵ_4 .

The boundary conditions consists of a no-flux condition along the line of symmetry and on the wing surface, and a far-field boundary condition on the outer boundary of the computational domain. Along the line of symmetry the pressure is extrapolated from the interior points while on the wing the normal momentum equation is used to extrapolate the pressure from the interior points. The far-field condition is enforced by specifying free-stream conditions on a large outer boundary such that the bow shock is captured as a part of the solution.

A modified Joukowski transformation[21] has been used to generate the grid in the ζ-η plane.

The solution is obtained by using a four-stage Runge-Kutta time stepping starting from initial conditions corresponding to the free-stream conditions which represent an impulsive entry of the wing into the uniform free-stream flow.

Applications to Supersonic Conical Sharp-Edged Wing Flows

In Figure 7, we show the results for a flat-plate sharp-edged delta wing with a grid size of 65x65 for M_∞=1.5, α=15^0 and β=70^0 . The cross-flow velocity, Figure 6.1, shows the leading-edge vortex and two shocks; a weak shock above the vortex at its inner boundary and a strong shock below the vortex. The latter is analogous to the flow in a convergent-divergent channel flow. The cross-flow Mach contours, Figure 6.2, and the surface pressure, Figure 6.3, clearly show the strong shock formed under the vortex. These results confirm Vorropoulos and Wendt observation[3] and our calculations using the integral equation approach. This case is indicated as Fig. 7 on the Miller-Wood diagram, Figure 2.

In Figure 8, we show the results for a flat-plate sharp-edged delta wing with a grid size of 65x65 for M_∞ = 2.4, α=19^0 and β=70^0 . The results clearly show the leading-edge vortex and a strong shock above the vortex at its inner boundary. This case is indicated as Fig. 8 on the Miller-Wood diagram, Figure 2.

In Figure 9, we show the results for a flat plate sharp-edged delta wing with a grid size of 29x39 for M_∞ = 2, α=10^0 and β=70^0 . The leading-edge vortex is captured and no shocks are captured. This case is indicated as Fig. 9 on the Miller-Wood diagram, Figure 2.

Figure 10 gives the three-dimensional solution for the case considered above (Figure 9) with a grid size of 36x29x39 which has the same resolution in the cross-flow planes as that of the conical solution (Figure 9). The three dimensional grid is generated by the modified Joukowski transformation at 36 chord stations. The results are shown at five chord stations of 0.053, 0.478, 0.829, 0.998 and 1.03. It is seen that the flow is conical on the wing except at the trailing edge and after. Moreover, it is seen that the trailing-edge vortex at the chord station x=1.03 is captured and it is of opposite strength to the leading-edge vortex. Obviously, a fine grid is required to obtain better resolution.

It is seen that the supersonic conical and three-dimensional solutions obtained by the finite-volume Euler solver for sharp-edged delta wings are consistent with the Miller-Wood flow-classification diagram for the regions where leading-edge separations exist. For these regions, the least level of dissipation, as long as it is sufficient to obtain a stable solution, produces consistent separated flows. Work is underway to check the solutions for the attached-flow regions, where the leading-edge is supersonic, and to quantitatively compare the computed results with the experimental data. Our preliminary comparison with the experimental data shows that the suction-pressure peak is overpredicted.

Applications to Supersonic Conical Round-Edged Wings

Figures 11-13 show the results for the supersonic conical solutions of a round-edged elliptic-section delta wing for M_∞=2, α=10^0, β=70^0 and δ=2^0 (δ is half the vertex angle of the cone in the plane of symmetry). The grid size in Figures 11 and 12 is 65x65 and the damping coefficients are (0.25, 0.004) and (0.05, 0.0008). The grid size in Figure 13 is 100x100 and the damping coefficients for part (A) are (0.25, 0.004) and for part (B) are (0.4, 0.0064).

Figures 11 and 12 show that separated and attached-flow solutions are produced depending on the level of dissipation. Figure 13 [parts (A) and (B)] shows that with a fine grid an attached-flow solution is obtained but the level of dissipation is substantially affecting the surface pressure. A growing bump in the surface pressure, on the inboard side of the shock, is noticed as the level of dissipation is increased. This bump in the surface pressure can be explained as a product of the vorticity shed from the curved shock (Crocco's theorem) and a separation bubble produced by the dissipation terms in the numerical scheme (analogous to the viscous terms in Navier-Stokes equations). In a coarse-grid solution with sufficient dose of dissipation the bump grows fast and takes over the shock region producing a leading edge separation. Although the attached-flow solution is the solution to be produced by the Euler equations, the separated-flow solution resembles the real flow and the Navier-Stokes solution for this case. It is obvious that a reliable solution (an attached-flow solution) would be obtained with a very fine grid, a small level of dissipation and a high-accuracy computer[21] (at least 64-bit word length). Consequently, the computational cost will increase and impose a serious limitation on the practical application of Euler equations to real life aerodynamics with complex geometry.

Currently, we are looking at the problem of

non-uniqueness of the modified differential equation of the difference equation of the scheme. It is possible that we are dealing with a singular perturbation problem where a small parameter is multiplying the highest derivative (second- and fourth-order dissipation terms) with insufficient boundary conditions on the velocity component along the wing surface. The question to be answered is: Could we render the numerical solution unique by imposing artificial boundary conditions at the wing surface and still use the coarse grid to obtain solutions corresponding to the real flow? Another related question is: Can we obtain an attached flow solution keeping the damping coefficients fixed, starting with a coarse grid and refining the grid during the time stepping?

Work in Progress

It is obvious from the solutions obtained so far that the dissipation level is substantially affecting transonic and supersonic flow solutions with leading-edge separations. Since the vortical-flow solutions obtained from the integral-equation approach are dissipation free and does not require large computational domain and since Euler equation solutions are better in capturing shocks and modeling the large entropy production across strong shocks, the logical approach to obtain a reliable solution, over a wide range of Mach numbers with an acceptable computational cost, is to combine the two techniques into a hybrid solver. This is achieved by splitting the flow-vector field into two components - a vortical flow field and a flow field due to the remaining disturbances. The former is calculated from the integral-equation technique while the latter is calculated from a modified Euler-equation technique where most of the vortical flow field is known a priori.

Concluding Remarks

We have presented two computational techniques for the transonic and supersonic vortex-dominated flows - an integral equation technique and a finite-volume Euler technique. Results are presented for the two techniques and the advantages and disadvantages of each technique have been presented and discussed. Since the integral equation technique is based on the full potential equation its solution is limited to low transonic regimes. However, the integral equation technique does not require large computational domain. On the other hand, the finite-volume Euler technique is better in capturing shock waves but its solutions are affected by the numerical dissipation. A hybrid technique which combines both techniques has been proposed to obtain reliable solutions at acceptable computational costs.

Acknowledgement

This work has been supported by the Unsteady Aerodynamics Branch of NASA Langley Research Center under Grant No. NAG-1-648. Part of this work has also been supported under NASA Grant No. NAG-1-591.

References

1. Squire, L. C., Jones, J. G. and Stanbrook, A., "An Experimental Investigation of the Characteristics of Some Plane and Cambered 65° Delta Wings at Mach Numbers from 0.7 to 2.0," ARC R&M 3305, 1961.

2. Stanbrook, A. and Squire, L. C., "Possible Types of Flow at Swept Leading Edges," Aeronautical Quarterly, Vol. XV, February 1964.

3. Vorropoulos, G. and Wendt, J. F., "Laser Velocimetry Study of Compressible Effects on the Flow Field of a Delta Wing," AGARD CP 342, April 1983.

4. Miller, D. S. and Wood, R. M., "An Investigation of Wing Leading-Edge Vortices at Supersonic Speeds," AIAA Paper 83-1816, July 1983.

5. Miller, D. S. and Wood, R. M., "Lee-Side Flow Over Delta Wings at Supersonic Speeds," NASA, T.P. 2430, 1985.

6. Kandil, O. A., "Numerical Prediction of Vortex Cores from the Leading and Trailing Edges of Delta Wings," ICAS Paper 14.2, The 12th Congress of the International Council of the Aeronautical Sciences, Munich, FRG, October 1980.

7. Kandil, O. A., Chu, L. C., and Tureaud, "A Nonlinear Hybrid Vortex Method for Wings at Large Angle of Attack," AIAA Journal, Vol. 22, No. 3, March 1984, pp. 329-336.

8. Kandil, O. A. and Yates, E. C., Jr., "Computation of Transonic Vortex Flows Past Delta Wings-Integral Equation Approach," AIAA Paper 85-1582, July 1985. Also to appear in AIAA Journal, September 1986.

9. Minailos, A. N., "Calculation of Supersonic Flow Past Wings with Consideration of Tangential Discontinuities Shed from the Edges within the Scope of a Model Using a System of Euler Equations," Fluid Dynamics, Vol. 13, No. 1, January-February 1978, pp. 78-89.

10. Klopfer, G. H. and Nielsen, J. N. "Euler Solutions for Wings and Wing-Body Combination at Supersonic Speeds with Leading-Edge Separation," AIAA Paper 80-0126, January 1980.

11. Rizzi, A., Eriksson, L. E., Schmidt, W., and Hitzel, S. M. "Simulating Vortex Flows Around Wings," AGARD CP No. 342, April 1983, pp. 21.1-21.14.

12. Raj, P. and Sikora, J. A., "Free-Vortex Flows: Recent Encounters with an Euler Code," AIAA Paper 84-0135, January 1984.

13. Rizzi, A., "Three-Dimensional Solutions to Euler Equations with One Million Grid Points," AiAA Journal, Vol. 23, No. 12, December 1985, pp. 1986-1987.

14. Krause, E., Shi, X. G. and Hartwich, P. M., "Computation of Leading Edge Vortices," AIAA Paper 83-1907, July 1983.

15. Powell, K., Murman, E., Perez, E. and Baron, J., "Total Pressure Loss in Vortical Solutions of the Conical Euler Equations," AIAA Paper 85-1701, July 1985.

16. Murman, E., Powell, K. and Miller, D., "Comparison of Computations and Experimental Data for Leading Edge Vortices, Effects of Yaw and Vortex Flaps," AIAA Paper 86-0439, January 1986.

17. Newsome, R. W., "A Comparison of Euler and Navier-Stokes Solutions for Supersonic Flow Over a Conical Delta Wing," AIAA Paper 85-0111, Jan. 1985. Also AIAA Journal, Vol. 24, No. 4, April 1986, pp. 552-561.

18. Newsome, R. W. and Thomas, J. L., "Computation of Leading-Edge Vortex Flows," Vortex Flows Aerodynamics Conference, NASA Langley Research Center, Hampton, VA, October 1985.

19. Chakrvarthy, S. R. and Ota, D. K., "Numerical Issues in Computing Inviscid Supersonic Flow over Conical Delta Wings," AIAA Paper 86-0440, January 1986.

20. Kandil, O. A. and Chuang, A., "Numerical Dissipation Effects in Finite-Volume Euler Solutions for Conical Vortex Dominated Flows," *Proceedings of the International* Conference on Computational Mechanics, ICCM86 Paper No. K-8, Tokyo, Japan, May 1986.

21. Kandil, O. A. and Chuang, A., "Influence of Numerical Dissipation in Computing Supersonic Vortex-Dominated Flows," AIAA Paper 86-1073, May 1986.

22. Murman, E. M. and Rizzi, A., "Applications of Euler Equations to Sharp Edge Delta Wings with Leading Edge Vortices," AGARD Symposium on Application of Computational Fluid Dynamics in Aeronautics, Aux-En-Provence, France, April 1986.

23. Powell, K. G., Murman, E. M., Wood, R. M. and Miller, D. S., "A Comparison of Experimental and Numerical Results for Delta Wings with Vortex Flaps," AIAA Paper 86-1840-CP. June 1986.

24. Fuji, K. and Kutler, P., Numerical Simulation of the Leading-Edge Separation Vortex for a Wing and Strake Wing Configuration," AIAA Paper 83-1908, July 1983.

25. Newsome, R. W. and Adams, M. S., "Numerical Simulation of Vortical-Flow Over an Elliptical-Body Missile at High Angles of Attack," AIAA Paper 86-0559, January 1986.

26. Rizetta, D. P. and Shang, J. S., "Numerical Simulation of Leading Edge Vortex Flows," AIAA Journal, Vol. 24, No. 2, February 1986, pp. 237-245.

27. Thomas, J. L. and Newsome, R. W., Navier-Stokes Computations of Lee-Side Flows over Delta Wings," AIAA Paper 86-1049, May 1986.

28. Srinivasan, G. R., McCroskey, W. J., Baeder, J. D. and Edwards, T. A., "Numerical Simulation of the Tip Vortex on a Wing in Subsonic and Transonic Flows," AIAA Paper 86-1095, May 1986.

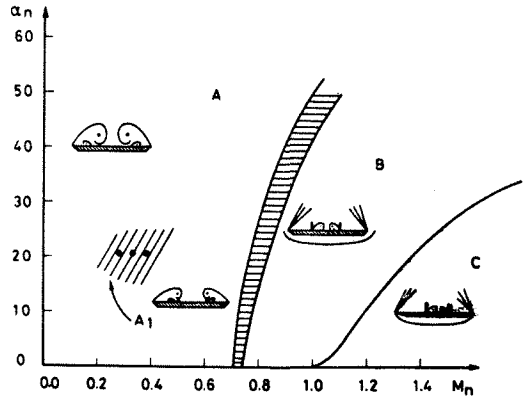

Figure 1. Stanbrook-Squire diagram with Vorropoulos and Wendt subregion (A_1), Reference 2 .

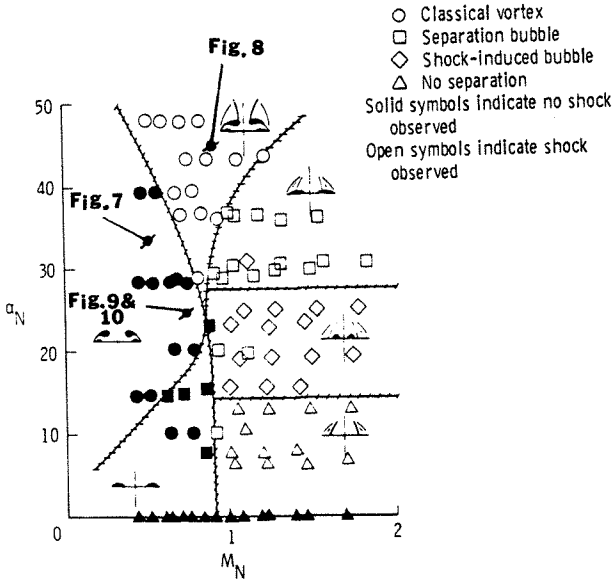

Figure 2. Miller and Wood Flow-Classification Diagram, Reference 5 .

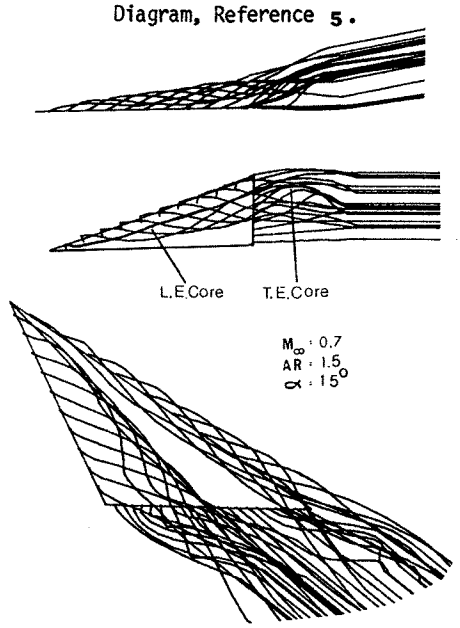

Figure 3. Typical solution of the leading- and trailing-edge free-vortex lines.

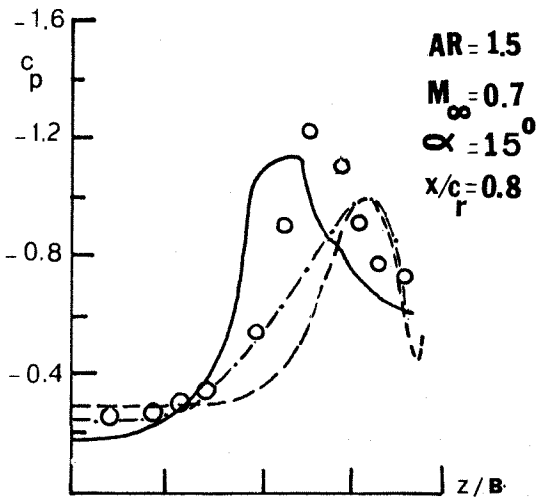

Figure 4. Surface pressure for a sharp-edged wing
---- Rizzi, et. al[11], 21x15x65, O-O transfinite grid
— · — FL057 used by authors
—— Kandil and Yates[8], Integral Equation
0 Experiment (Ref. 11)

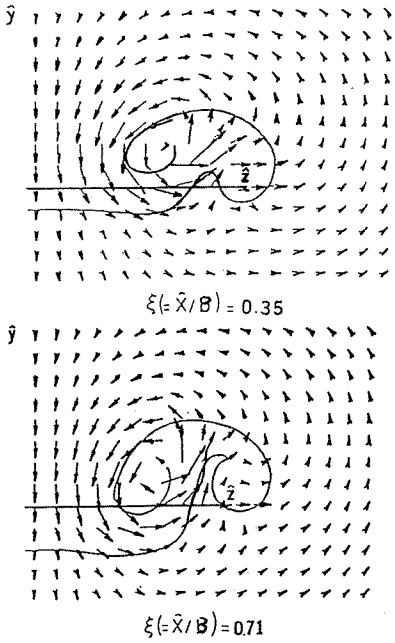

Figure 5. Cross-flow velocity and free-vortex sheets behind the trailing edge in planes normal to the wind direction.

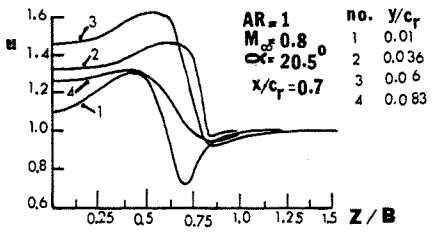

Figure 6. Spanwise variation of the axial velocity at different heights above the leeward side.

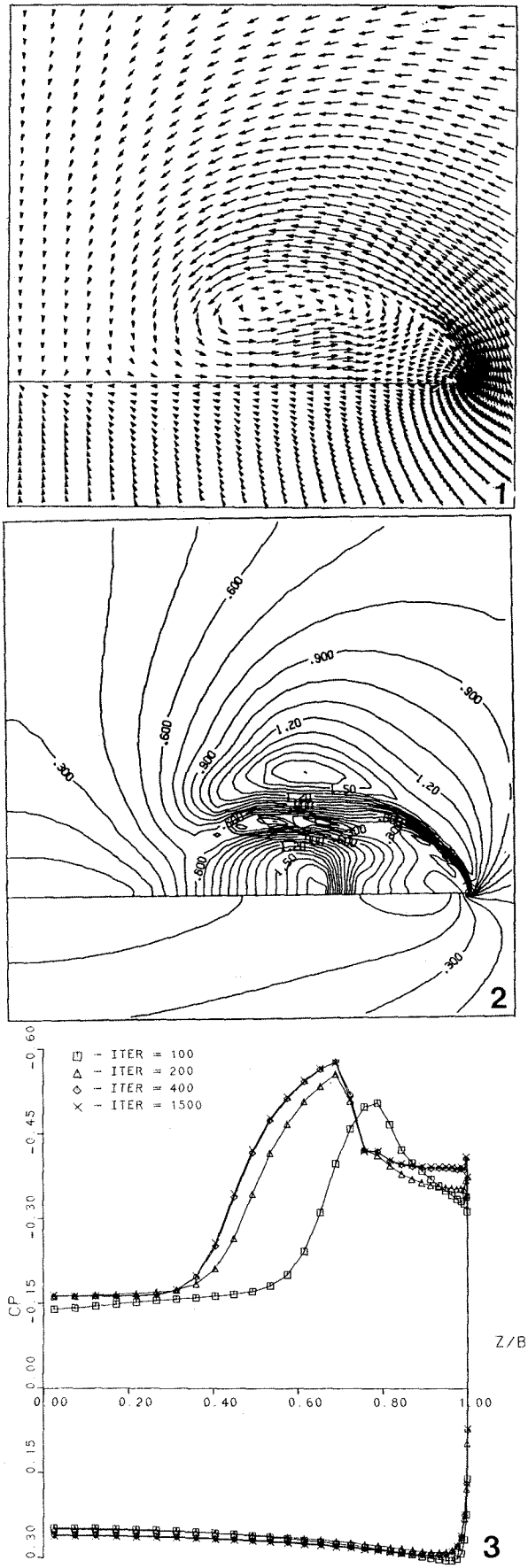

Figure 7. Results for a separated-flow solution of a sharp-edged wing, ε_2=0.12, ε_4=0.0012, 65x65 grid, α=15^0, M_∞=1.5, β=70^0, (1) cross-flow vel., (2) cross-flow Mach, (3) surface pressure.

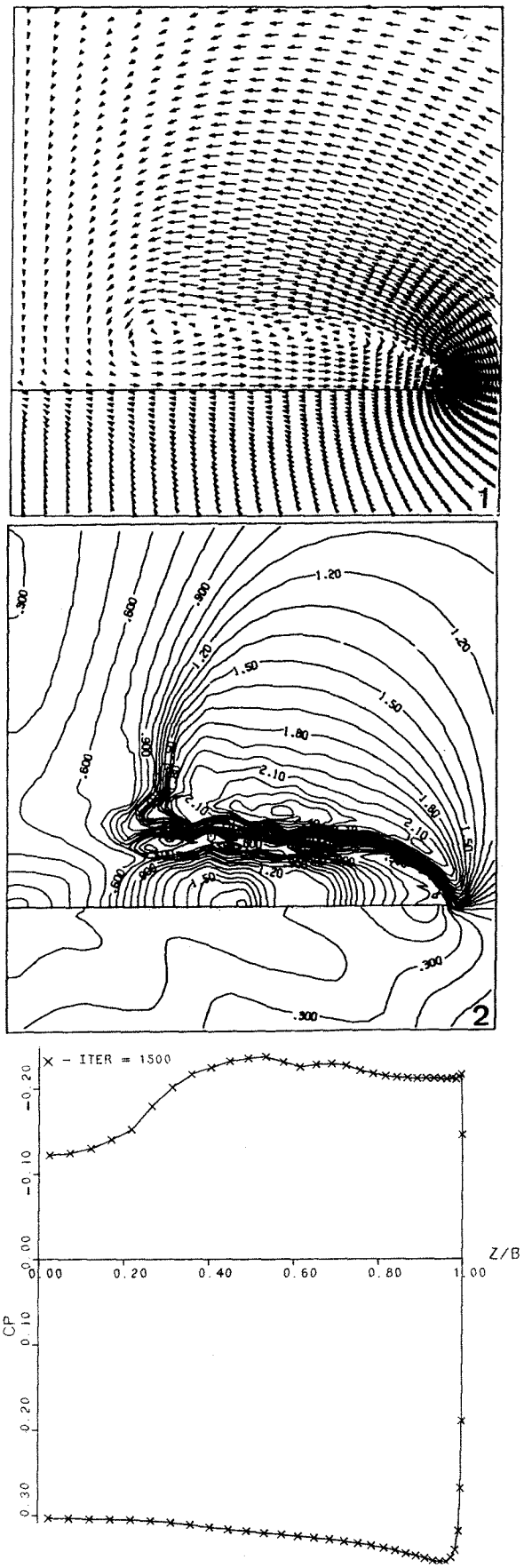

Figure 8. Results for a separated-flow solution of a sharp-edged wing, ε_2=0.1, ε_4=0.0008, 65x65 grid, α=19^0, M_∞=2.4, β=70^0, (1) cross-flow vel., (2) cross-flow Mach, (3) surface pressure.

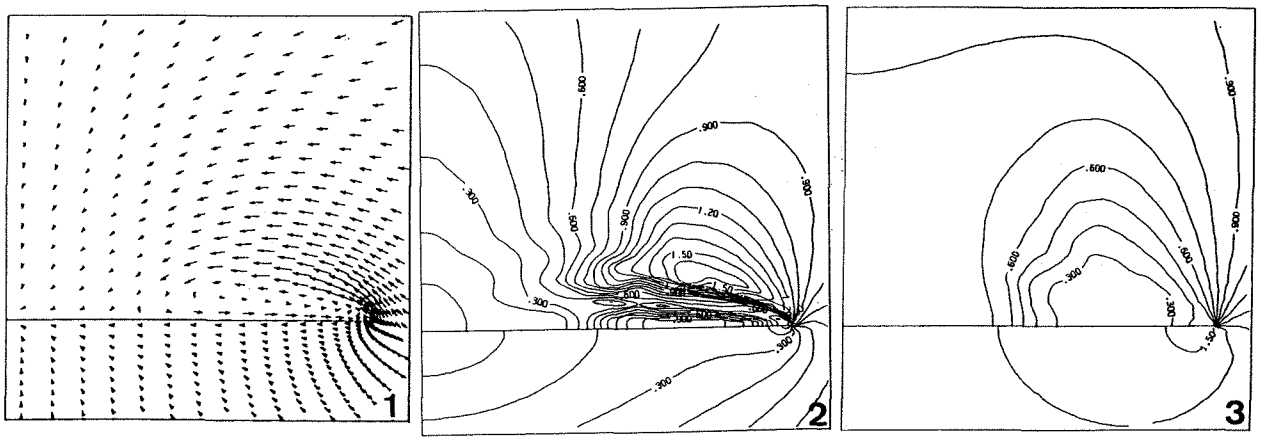

Figure 9. Results for a separated-flow solution of a sharp-edged wing (conical-flow solution), ε_2=0.1, ε_4 = 0.004, 29,x39 grid, α=10^0, M_∞=2, β=70^0, (1) cross-flow vel., (2) cross-flow Mach, (3) static-pressure.

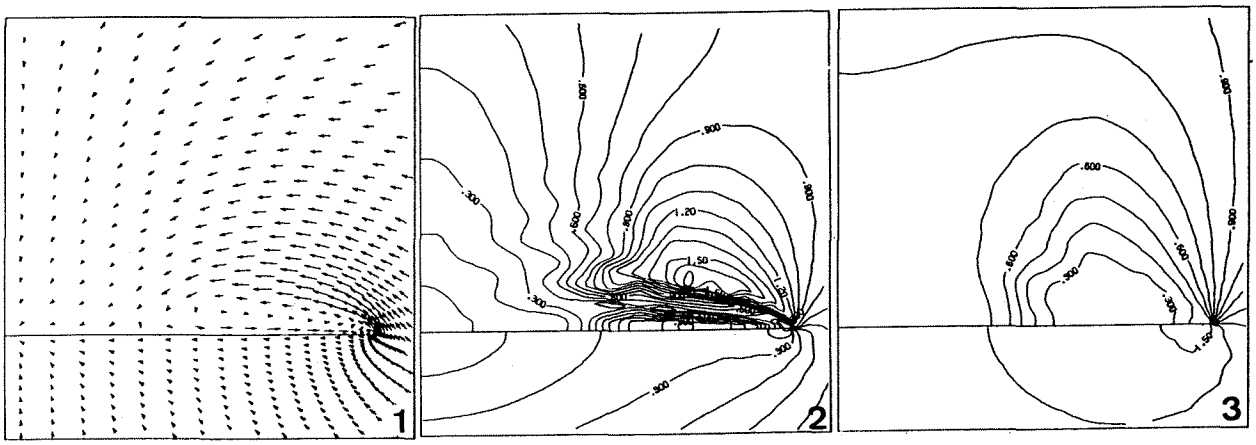

X = 0.053

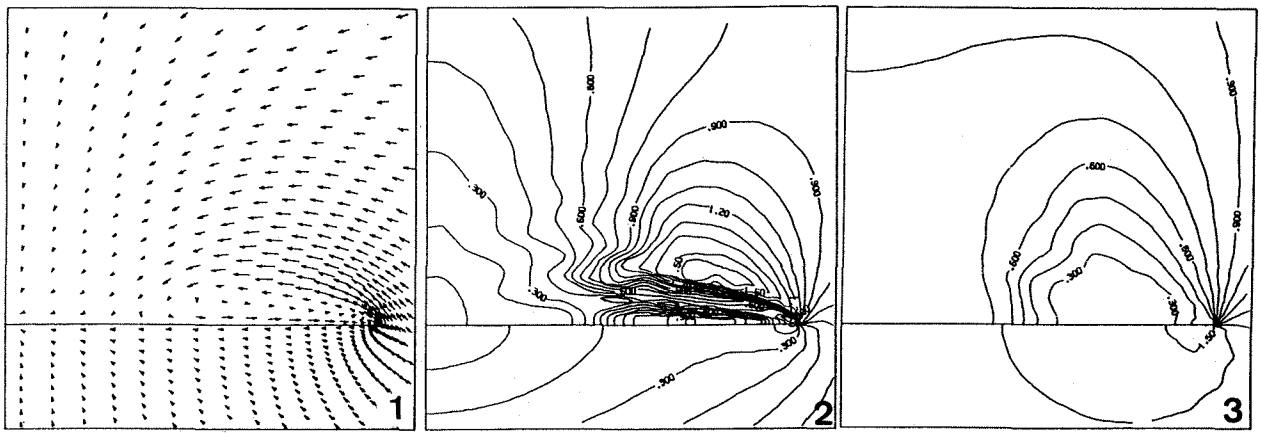

X = 0.478

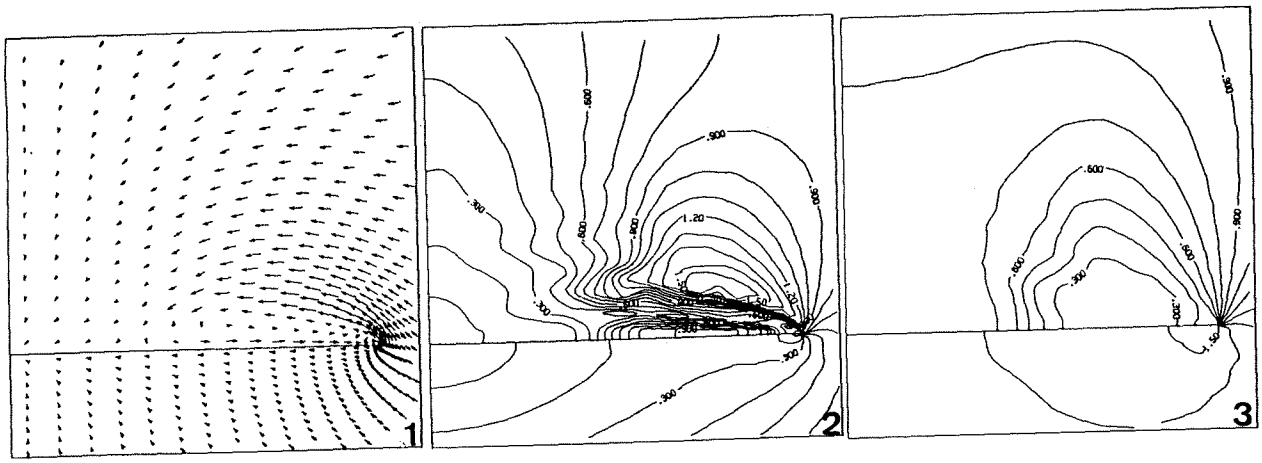

X =0.829

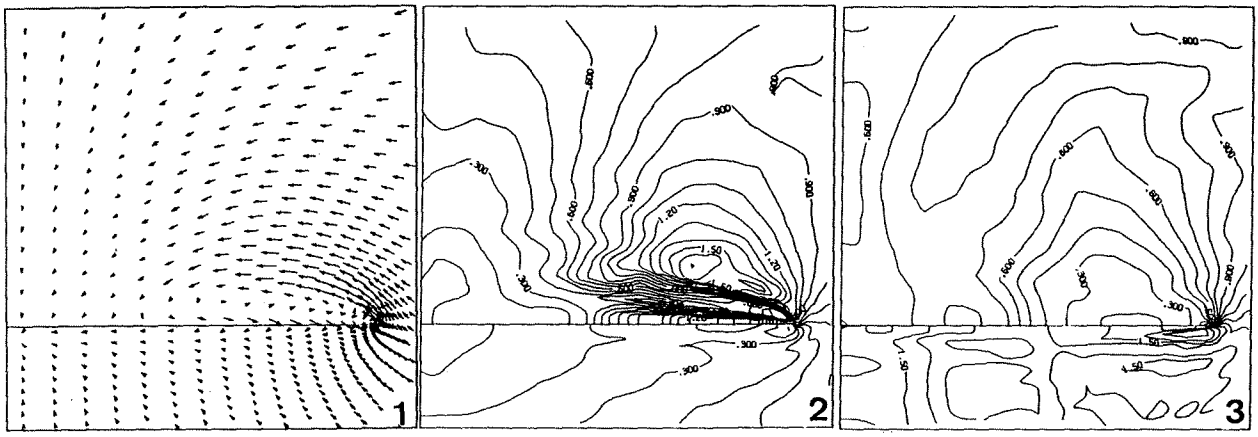

X = 0.998

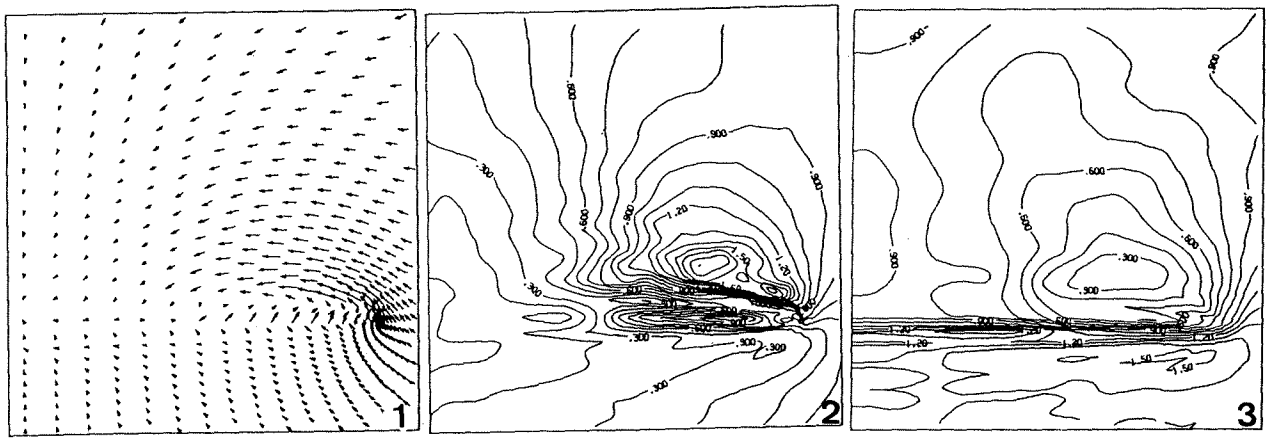

X = 1.03

Figure 10. Results for a separated-flow solution of a sharp-edged wing at different chord stations (three-dimensional solutions), ε_2=0.1, ε_4=0.0016, 36x29x39 grid, $\alpha=10^0$, $M_\infty=2$, $\beta=70^0$, (1) cross-flow vel., (2) cross-flow Mach, (3) static-pressure.

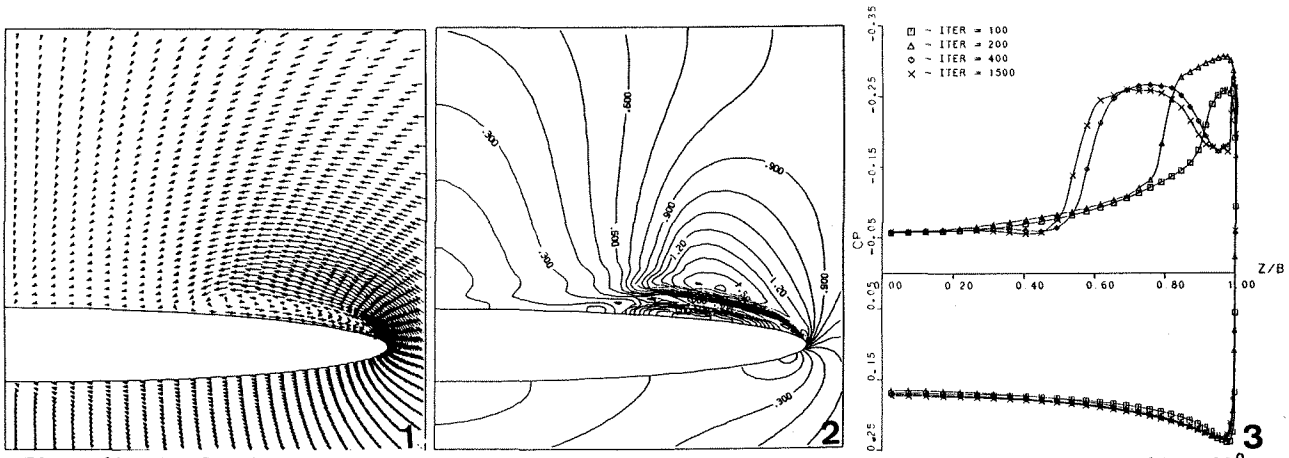

Figure 11. Results for a separated flow solution of a round-edged wing, ε_2=0.25, ε_4=0.004, 65x65 grid, α=10^0, M_∞=2, β=70^0, δ=2^0, (1) cross-flow vel., (2) cross-flow Mach, (3) surface pressure.

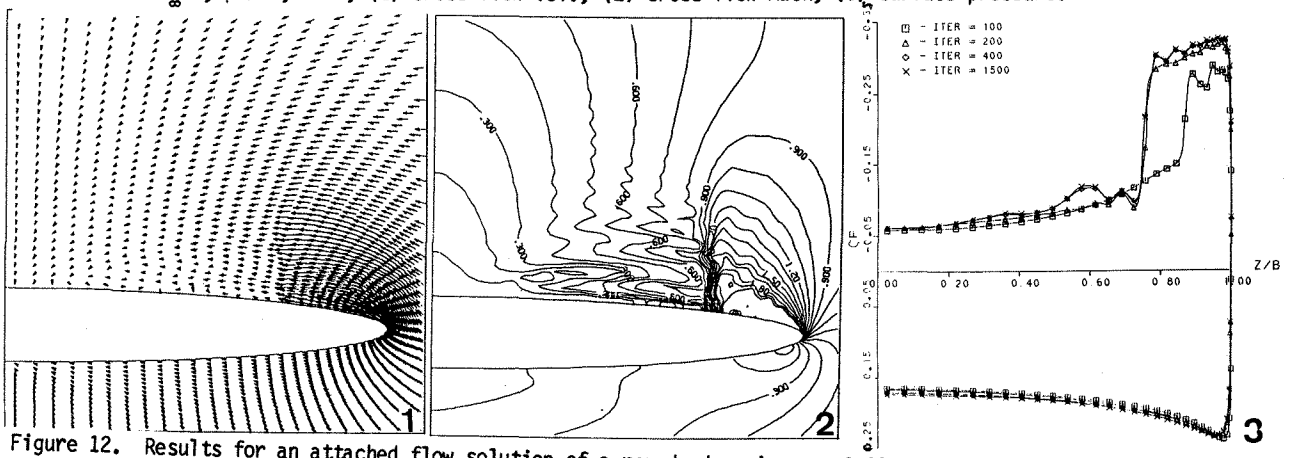

Figure 12. Results for an attached flow solution of a round-edge wing, ε_2=0.005, ε_4=0.0006, 65x65 grid, α=10^0, M_∞=2, β=70^0, δ=2^0, (1) cross-flow vel., (2) cross-flow Mach, (3) surface pressure.

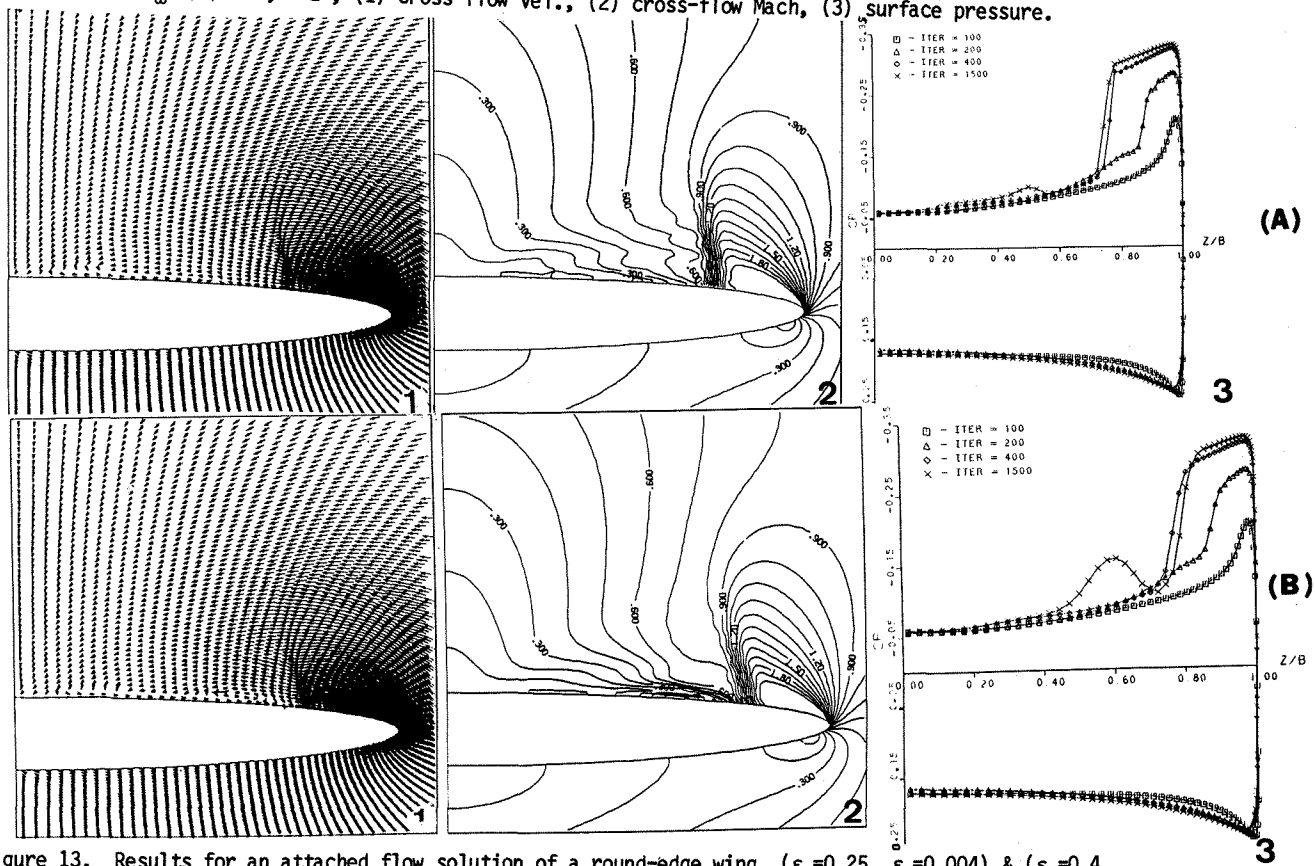

Figure 13. Results for an attached flow solution of a round-edge wing, (ε_2=0.25, ε_4=0.004) & (ε_2=0.4, ε_4=0.0064), 100x100 grid, α=10^0, M_∞=2, β=70^0, δ=20^0, (1) cross-flow vel., (2)cross-flow Mach, (3)surface pressure.